Exfoliation Corrosion Behavior of 2B06 Aluminum Alloy in a Tropical Marine Atmosphere

Z.Y. Cui, X.G. Li, K. Xiao, C.F. Dong, L.W. Wang, D.W. Zhang, and Z.Y. Liu

In this study, corrosion behavior of 2B06 aluminum alloy was investigated after exposure to a tropical marine atmosphere for up to 4 years. After 6 months, the specimen showed exfoliation corrosion as well as rapid increase in thickness loss and corrosion rate. Exfoliation corrosion was found to initiate from hydrogen-assisted intergranular cracks and propagate extensively due to the wedge effect of the corrosion products. During the exposure test, corrosion on the groundward surface was considerably more severe than that on the skyward surface, which could be attributed to the different exposure conditions on the two surfaces.

1. Introduction

Due to the high mechanical properties and low density, $2 \times \times \times$ series aluminum alloys have been extensively used as structural materials in the fields of transportation, building construction, electrical engineering, aircraft, and aerospace (Ref 1, 2). Aluminum's great affinity to oxygen allows the formation of oxide films with desirable properties in terms of adhesion, continuity, and corrosion resistance (Ref 3). In many natural environments, therefore, aluminum alloys show excellent resistance to atmospheric corrosion. However, when they are exposed to marine atmosphere, the presence of chloride ions would destroy the passive oxide films and induce corrosion attacks.

Recently, corrosion behavior of aluminum alloys in various atmospheres has been reported in some literatures (Ref 4-11). The corrosion morphology of aluminum alloy was usually characterized as localized and took the forms of pitting corrosion, intergranular corrosion, stress corrosion cracking (SCC), or exfoliation corrosion. Previous studies on atmospheric corrosion of aluminum alloys have been primarily focused on pitting, intergranular corrosion, and SCC, while few have concerned the exfoliation corrosion (Ref 12-14). Exfoliation corrosion often occurs on the $2 \times \times \times$ series aluminum alloys with preferential anodic sites along the grain boundary which increases the material's sensitivity to corrosion. According to Sprowls, the forged truck wheels made of 2024-T4 aluminum alloy exfoliated severely in only 1 or 2 years in the northern United States, where deicing salts were used on the

highways during the winter season (Ref 12). Sun et al. (Ref 13) investigated the exfoliation behavior of extruded 2024-T4 aluminum exposed to atmosphere in several locations of China and suggested that increasing temperature or the Cl$^-$ amount caused more serious exfoliation on specimen. The corrosion products between the uncorroded thin sheets of extruded 2024-T4 were all composed of γ-Al(OH)$_3$ and α-Al$_2$O$_3$·3H$_2$O, which exerted a wedging pressure to pry the neighboring sheets apart.

The mechanisms underlying exfoliation corrosion have been widely investigated by many researchers (Ref 15-20). However, there is no consensus so far in determining the susceptibility of aluminum alloys to exfoliation corrosion. A number of factors are believed to play important roles in exfoliation corrosion of aluminum including intergranular corrosion susceptibility (Ref 18), role of wedge effect on the grain lift-out due to the precipitation of corrosion scales (Ref 15) and role of hydrogen embrittlement (Ref 19). In general, exfoliation corrosion is developed from intergranular corrosion and alloys which have higher susceptibility to intergranular corrosion are more prone to exfoliation corrosion (Ref 17). Intergranular corrosion is attributed to the difference in the electrochemical potentials between the bulk of the grain and the grain boundaries where intermetallic phases precipitate (Ref 1). Once the intergranular corrosion occurs, corrosion products will form at the tip of intergranular cracks, producing considerable wedging forces between the grain matrices. The increased wedging volume forces the grain matrices apart and finally leads to exfoliation (Ref 13). Proposed by Marlaud (Ref 21, 22), another reasonable mechanism called intergranular fracture-induced damage (IFD) suggested that the uptake of hydrogen in the material at or close to the grain boundary could also result in the grain boundary fracture. According to this theory, the high concentration of segregated hydrogen at or close to the interface of grain boundaries could lead to the recombination of hydrogen atoms into molecular H and/or to the hydrogen-assisted intergranular decohesion. The key difference between the two mechanisms is whether the stress causing the crack formation is due to the volumic effect of corrosion products or the effect of hydrogen. In actual exposure test, however, what really induces and controls the exfoliation behavior of aluminum alloy has not been properly understood. Therefore, a better knowledge of

Z.Y. Cui, X.G. Li, K. Xiao, C.F. Dong, D.W. Zhang, and Z.Y. Liu, Corrosion and Protection Center, University of Science and Technology Beijing, Beijing 100083, China; and L.W. Wang, Pipeline Research Institute of China National Petroleum Corporation, Langfang 065000, China. Contact e-mail: lixiaogang@ustb.edu.cn.
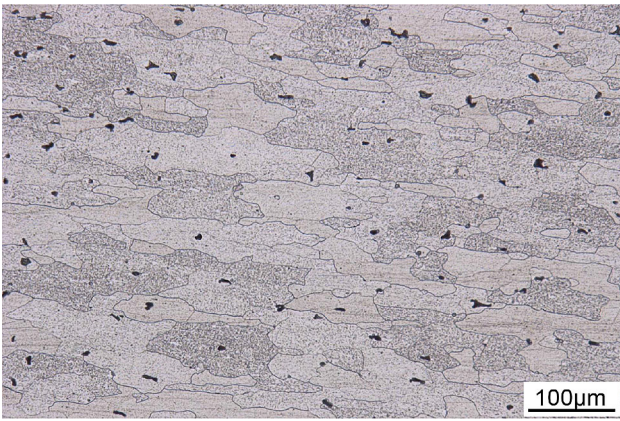
**Fig. 1** Microstructure of the longitudinal section (L/ST plane) of 2B06 aluminum alloy

exfoliation corrosion in aluminum alloy exposed to marine atmosphere is essential for any practical application.

In this work, the corrosion behavior of 2B06 aluminum is studied after exposing to a tropical marine atmosphere for 4 years. The initiation and evolution of exfoliation corrosion have been particularly discussed.

2. Experimental

2.1 Materials Preparation

The materials used in this study were the 2B06 aluminum alloys (China brand) which contained (in mass%) 3.8-4.3Cu, 1.7-2.3 Mg, 0.4-0.9Mn, 0.3Fe, 0.2Si, 0.05Zn and Al. The microstructure of the longitudinal section (L/ST plane) was observed via an stereology microscope (KEYENCE VHX2000)
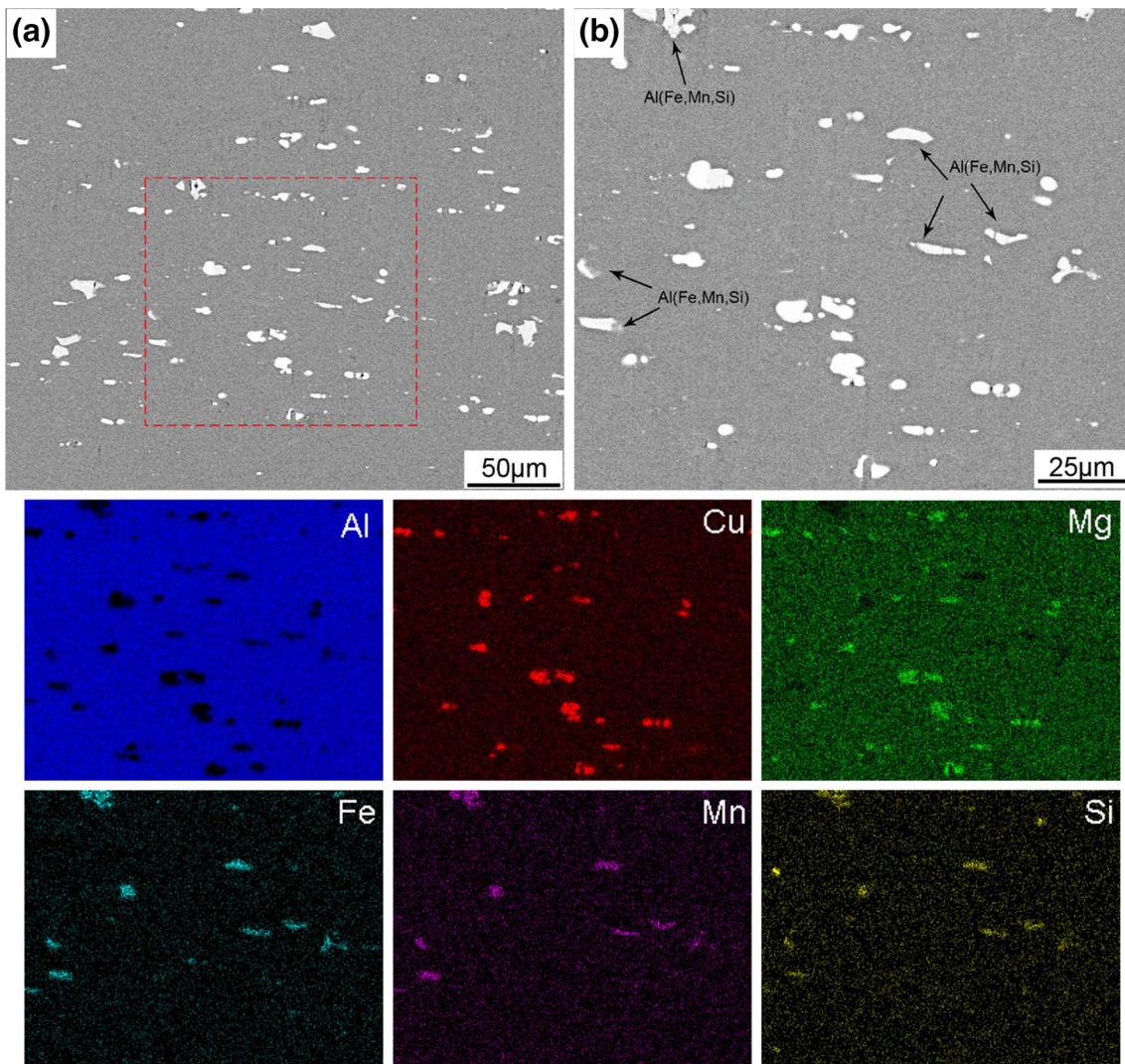

Fig. 2 SEM observation and element distributions of the intermetallic particles in 2B06 aluminum alloy (b is the magnification of the marked area in a)

Table 1 Climatic parameters and atmospheric pollutants of Xisha Islands during 4 years exposure

Exposure site	Location	Max. temperature	Min. temperature	Average temperature	Max. RH	Min. RH	Average RH
XiSha	112°20′E, 16°50′N	33.3 °C	20.1 °C	27 °C	94%	61%	77%

TOW, h/year	Rainfall, mm/year	Cl$^-$ deposition rate, mg/m^2 day	SO$_2$ deposition rate, mg/m^2 day	Sunshine, h/year	pH of rain	Distance to sea
2562 (τ_4)	1526	112.68 (S$_2$)	<0.1 (P$_0$)	2675	6.5	100 m
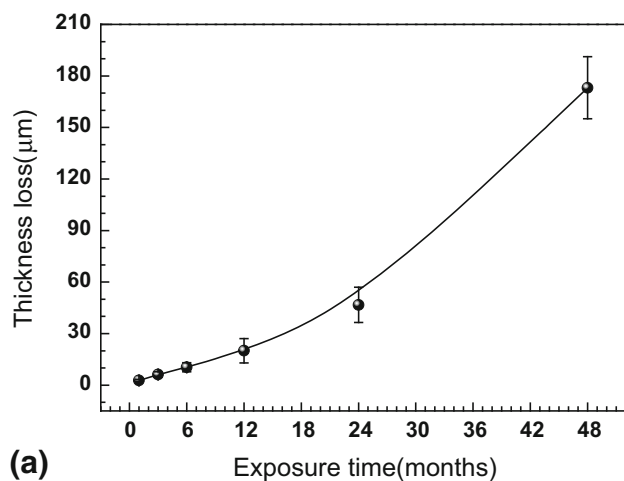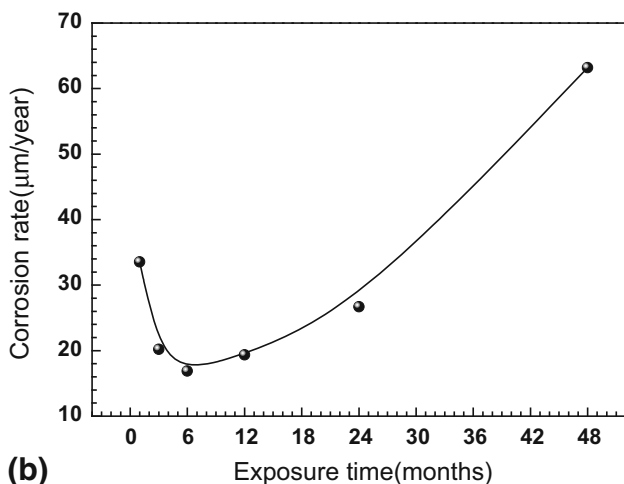
Fig. 3 Thickness loss and corrosion rate of 2B06 aluminum alloy during the exposure test: (a) thickness loss, (b) average corrosion rate
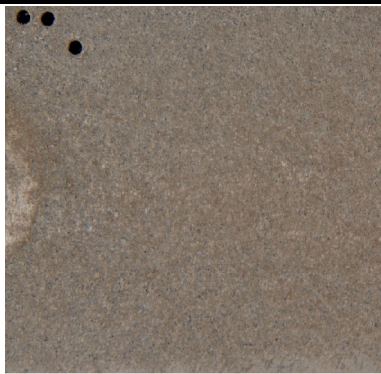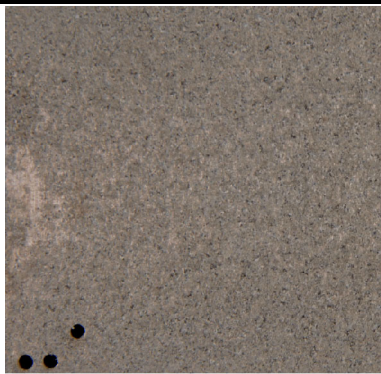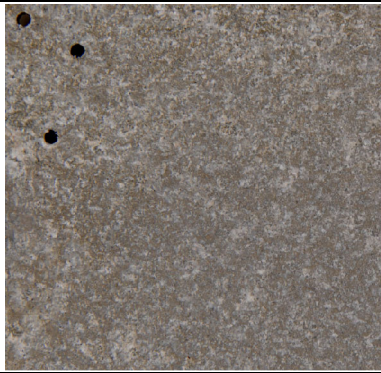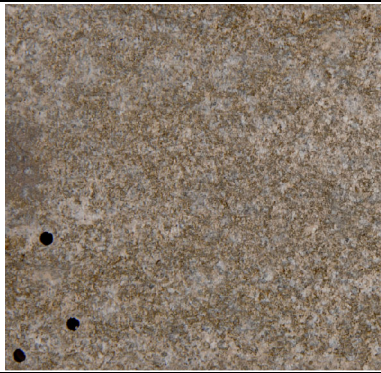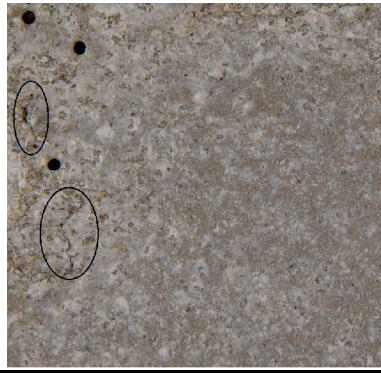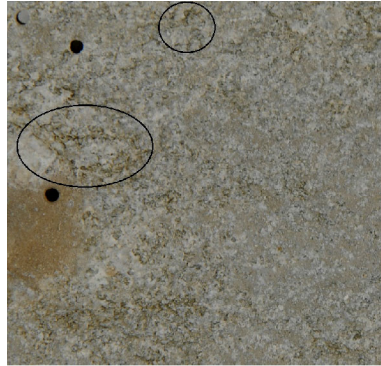
after etching in Keller's reagent (1 mL HF + 1.5 mL HCl + 2.5 mL HNO$_3$ + 95 mL H$_2$O) (Fig. 1). It showed that the grain structure was highly elongated parallel to the sample surface with some second phase particles located in the interior of grains and grain boundaries. The distributions and compositions of the intermetallic (IM) particles were examined with scanning electron microscope (SEM, Quanta 250) and energy dispersive x-ray spectroscopy (EDS) techniques. Figure 2 shows that the IM particles are mainly consisted of two phases: the elongated particles are Al (Fe, Mn, Si) phases (marked by arrows in Fig. 2b); and the rest of the particles, composing of elements Al, Cu, and Mg, is identified as S-phase (Al$_2$CuMg).

2.2 Field Exposure Test

Prior to the exposure test, all specimens (100 mm × 50 mm × 5 mm) were ground down to 800 grit and degreased by acetone, followed by cleaning in ethanol. The original weights and the surface area (S) of the specimens were then measured. Subsequently, the specimens were installed on a test rack with a inclination angle of 45° horizontal to the sky and facing south on Xisha islands (112°20′E, 16°50′N). The test duration was 4 years (Dec 2007-Dec 2011). Four replicate metal samples were retrieved from the exposure site after 1, 3, 6, 12, 24, and 48 months. Three of them were used to determine the average weight/thickness loss of the specimen, while the other one was used to analyze the corrosion morphology and corrosion products.

Table 1 lists the environmental parameters and atmospheric pollutants measured at Xisha Islands during the exposure, as well as the atmosphere classifications based on ISO 9223 (Ref 23). The average temperature in Xisha marine atmosphere was 27 °C with the maximum temperature increasing up to 33.3 °C and the minimum temperature reducing to 20.1 °C which was also a relatively high temperature. The extreme relative humidity (RH) values oscillated between 61 and 94% with a mean value of 77%. Time of wetness, which was defined as the period during which a metallic surface was covered by adsorptive and/or liquid film of electrolyte, was another important factor that affects the corrosion behavior of metals in atmosphere. Schindelholz (Ref 24) summarized that the TOW determination methods represented in literature and practice could be categorized by the way in which TOW was treated—either as an environmental parameter or as a surface parameter. However, both the two kinds of methods including ISO 9223 and other indirect electrode sensors had their limitations (Ref 25-27). In this work, the TOW was treated as an environmental parameter and was calculated according to ISO 9223, which defines TOW as the time during which the RH of the ambient environment is greater than 80% at temperatures above 0 °C. With this method, the approximate TOW in Xisha islands was 2562 h/year which belonged to the classification of τ_4 (Ref 23). As for the corrosive species precipitated on the samples, the Cl$^-$ and SO$_2$ deposition rates were considered and measured using the method given by ISO 9225 (Ref 28). The Cl$^-$ deposition rate was determined by the wet candle method, and the SO$_2$ deposition rate was determined using alkaline surfaces of porous filter plates saturated by a solution of sodium carbonate. According the results, the annual average deposition rate of chloride was 112.68 mg/m^2 day, which was classified to the S$_2$ (Ref 23). Meanwhile, the precipitation of SO$_2$ was less than 0.1 mg/m^2 day and the rain had a near-neutral pH of 6.5 because of no heavy industry existed at the exposure site.

Table 2 Macroscopic corrosion morphologies of 2B06 aluminum during the exposure test

	Skyward surface	Groundward surface
1 month		
12 months		
24 months		
48 months		

2.3 Thickness Loss Measurement

Corrosion products on the retrieved specimens were chemically removed by pickling in the solution (50 mL H_3PO_4 + 20 g CrO_3 + 1L H_2O) for 10 min at 80-100 °C. After that, the specimens were sequentially rinsed with distilled water, dried in warm air, and then weighed to obtain their final weights (w_1). The weight loss was calculated as follows: $C = w_0 - w_1$, where C is the weight loss of the metal due to corrosion (g), w_0 is the original weight (g), and w_1 is the final weight (g). The thickness loss (μm) was obtained from the equation:
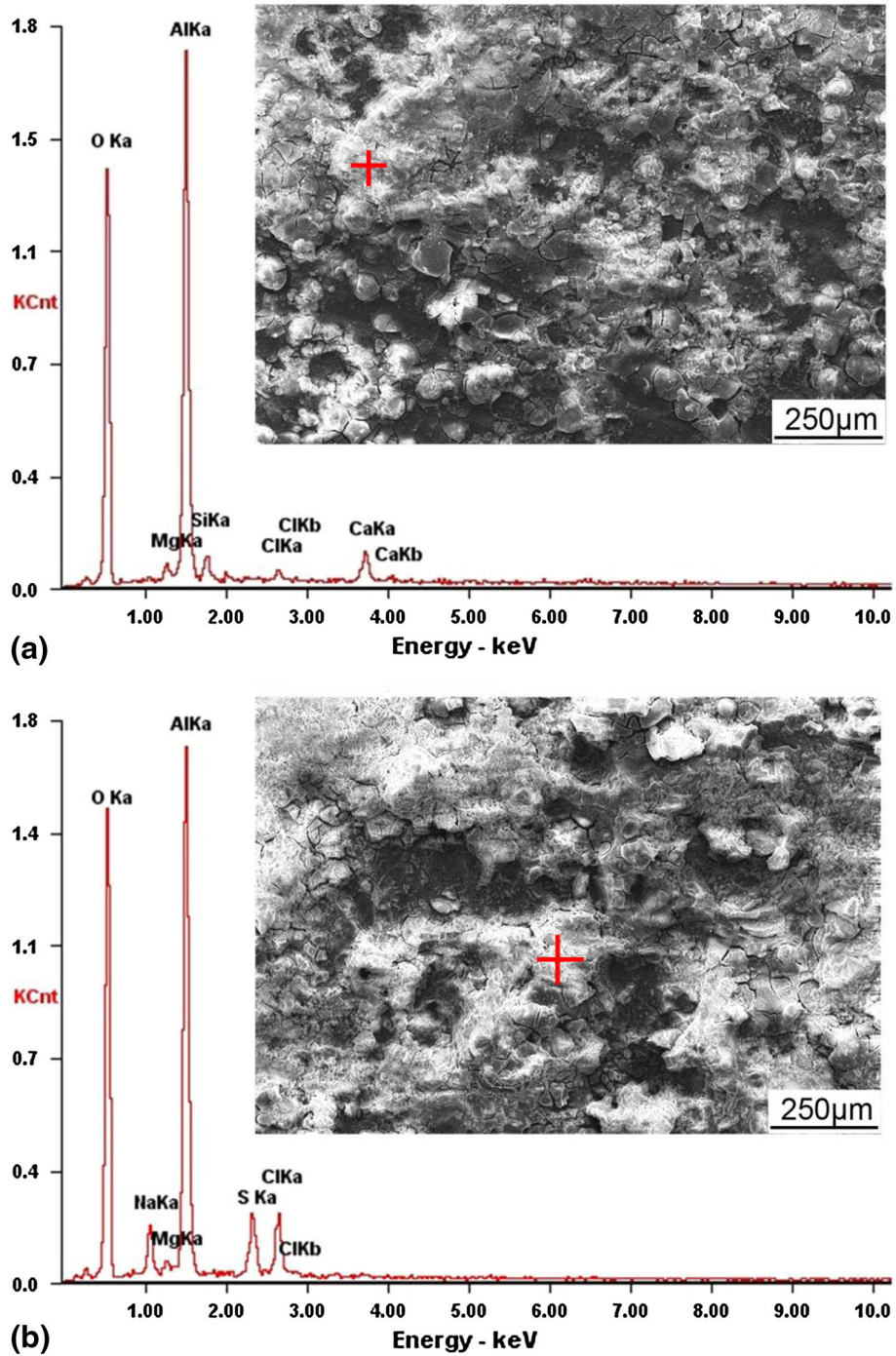
Fig. 4 Surface morphologies of 2B06 aluminum after exposure for 1 month (a) and 24 months (b) observed by SEM as well as the chemical composition of the marked site determined by EDS

$$d = \frac{C_t \times 10^4}{\rho S} \qquad \text{(Eq 1)}$$

In which, C_t is the weight loss (g), ρ is the density of aluminum, and S is the exposed area (cm^2). Therefore, the average corrosion rate of the aluminum alloy after different exposure time was calculated by the equation in Ref 29:

$$V_n = \frac{12(d_n - d_{n-1})}{t_n - t_{n-1}}, \qquad \text{(Eq 2)}$$

where V_n is the corrosion rate (μm/year), d_n is the thickness loss (μm), t is the exposure time (month), and n is the period of exposure ($n = 1, 2, 3, 4, 5$, and 6 refer to the samples exposed for 1, 3, 6, 12, 24, and 48 months, respectively).
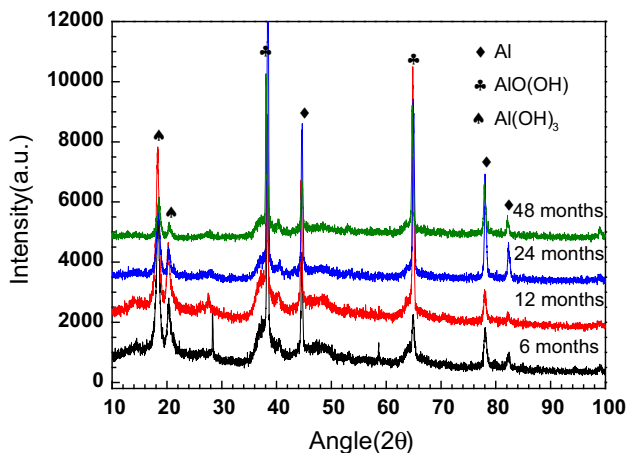
Fig. 5 XRD patterns of the corrosion products formed on 2B06 aluminum alloy after different exposure time

2.4 Characterization of Corrosion Morphologies and Corrosion Products

After exposure test, the macroscopic morphologies of 2B06 aluminum were observed by a Nikon D200 digital camera. The microscopic morphologies of the exposed samples with and without corrosion products were observed via SEM (Quanta 250). Elemental composition of the corrosion product layer was obtained by EDS. Phase identification was determined by x-ray diffraction (XRD, Rigaku Dmax-rc) and analyzed with Jade 5.0 software.

3. Results

3.1 Thickness Loss and Corrosion Rate

Figure 3 shows the thickness loss (a) and the corrosion rate (b) of 2B06 aluminum alloy during the 4-year exposure in Xisha atmosphere. The increase in thickness loss as a function of the exposure time can be divided into two stages: the initial 6 months during which the thickness loss grows slowly, and the rest of the exposure period which shows a more rapid, parabolic growth of the thickness loss. This phenomenon can be clearly explained by the variation of corrosion rate during the exposure test (Fig. 3b). From 1 month to 6 months, corrosion rate of 2B06 aluminum decreases from 33.5 to 16.9 μm/year. On the contrary, a significant acceleration of the corrosion rate can be observed after 6 months of exposure, indicating that the specimen has suffered severe deterioration in this stage. Typically, corrosion rate after 1 year of exposure is usually used to characterize the corrosivity level of the material at a certain exposure location. In Xisha islands, corrosion rate of 2B06 aluminum after exposure for 1 year is 20.05 μm/year (54.74 g/m^2 year) which is much higher than the 2××× aluminum alloys in salt lake (Ref 4), industrial, and costal atmospheres (Ref 5) in China.

3.2 Surface Appearances

Table 2 shows the macroscopic appearances of the samples' surfaces prior to the removal of corrosion products, after exposing for 1, 12, 24, and 48 months. After 1 month of exposure, both the skyward and the groundward surfaces of the

specimen are covered with gray corrosion products, and the original metallic luster is lost. As the exposure time increases to 12 months, more corrosion products can be observed, forming a thick layer. At this point, no visible exfoliation is detected with naked eye on both surfaces of the samples. After exposure for 24 and 48 months, some obvious cracks and pores (marked with the black circles) appear on the specimen surface and the corrosion products begin to delaminate and fall off, indicating the occurrence of exfoliation corrosion. Comparing with the skyward surface, the groundward surface exhibits more severe deterioration as a result of less radiation by sun and minor removal of the aggressive pollutants by rain.

3.3 Corrosion Product Analysis

In Fig. 4, the skyward surface morphologies of 2B06 aluminum after 1 and 24 months of exposure observed by SEM and the chemical composition of the marked site was determined by EDS. It is seen that morphology of the corrosion product shows minimal change with longer exposure. The EDS spectra reveal the presence of Al, O, Mg, Si, Cl, Ca, Na, and S in the corrosion products. The elements Al and O are possibly from the corrosion scales such as Al_2O_3, $Al(OH)_3$, and $AlO(OH)$, and the rest of the elements are mainly from the deposited salt particles from marine atmosphere.

Figure 5 shows the XRD patterns of the corrosion products on 2B06 aluminum exposed for different time. The major crystalline phases are identified to be $AlO(OH)$ and $Al(OH)_3$ which are the principle corrosion products formed on aluminum after long-term atmospheric exposure (Ref 9).

3.4 Cross-Section Analysis

Cross-sectional morphologies of L/ST plane of 2B06 aluminum exposed for various time are shown in Fig. 6 in which the left side is the skyward surface and the right side is the groundward surface feature. After exposure for 1 month (Fig. 6a), a number of thin and long cracks are observed across the whole micrograph beneath the sample surface. All cracks are parallel to the metal surface and part of them are filled with corrosion products, while no trace of corrosion product can be discerned at the crack tip of some extremely thin cracks. In addition, the sign of intergranular corrosion, which may have occurred prior to the exfoliation, is also found on the groundward surface of the specimen. The cracks widen with increasing exposure time and some of the corrosion products fall off from the gap, leaving a vacuous crevice (Fig. 6b). As the exposure test continues, many non-corroded grains begin to peel off due to the wedge forces created by the precipitation of corrosion products which have higher molar volumes than the aluminum (Ref 30). After 24 months of exposure, even more severe exfoliation can be observed, especially on the groundward surface where the metal matrix is swelled or pried open by corrosion scales (Fig. 6d).

As the exposure test lasts for 48 months, exfoliation of 2B06 aluminum exhibits qualitative change where the corroded layer can be clearly seen by naked eyes (Fig. 7). Exfoliation traces are visible on the groundward surface of the specimen after 24 months of exposure (Fig. 7a), indicating the occurrence of severe exfoliation corrosion. On the sample exposed for 48 months, the groundward surface shows more serious deterioration to the depth of 2.1 mm, almost half of the sample thickness (5 mm) (Fig. 7b). In this case, the mechanical strength and service life of aluminum have decreased significantly and the materials may experience sudden risks.
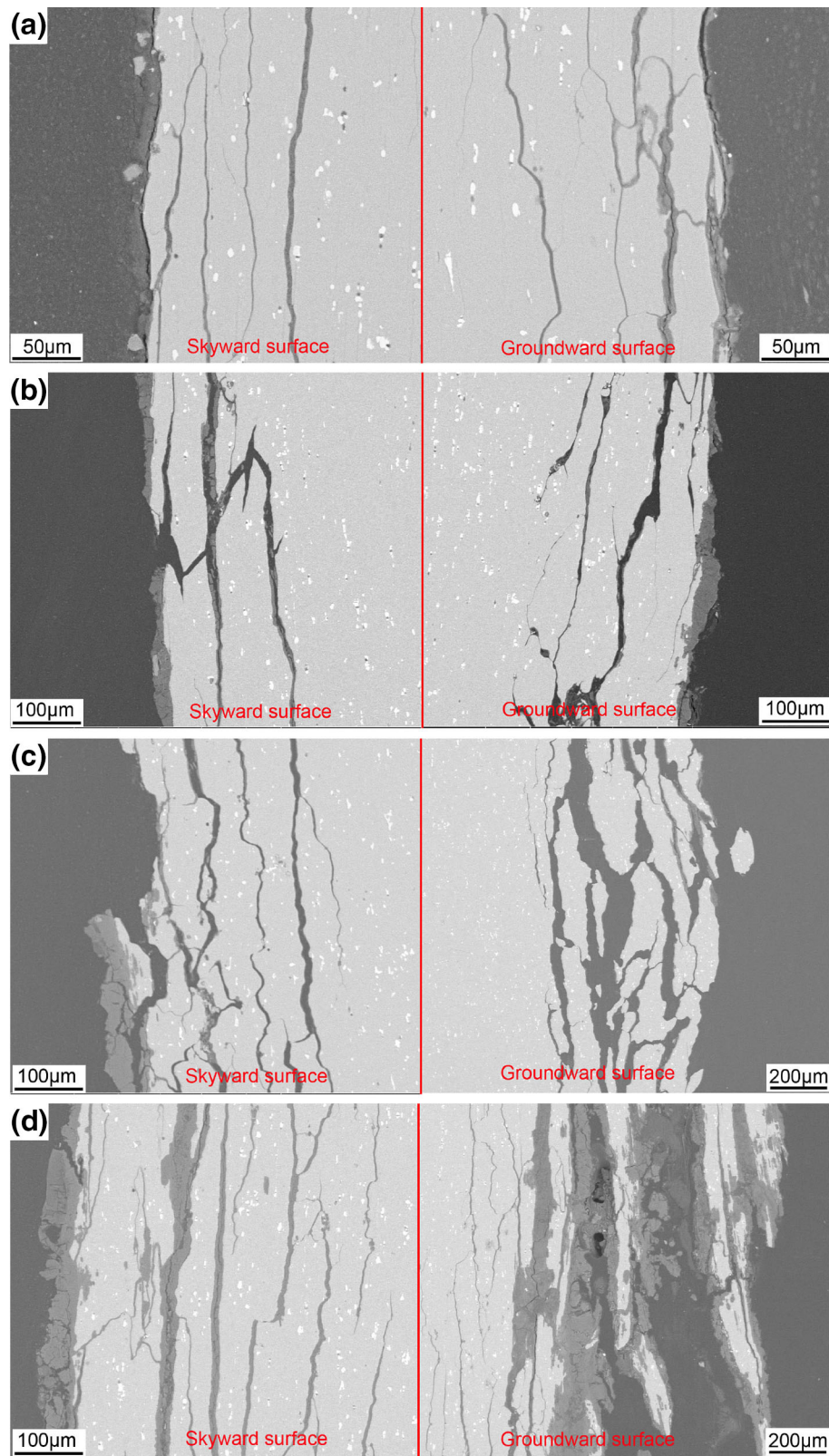
Fig. 6 Microscopic cross-sectional morphologies of L/ST plane of 2B06 aluminum exposed for various periods: (a) 1 month; (b) 6 months; (c) 12 months; (d) 24 months

A statistical analysis of the average corrosion depth, measured from the cross sectional surfaces, is shown in Fig. 8. It appears that the exfoliation layer begins to enlarge after 6 months of exposure, which agrees with the corrosion rate in Fig 3(b). Noticeably, the mean depth of the corrosion on the groundward surface is higher than the skyward surface and
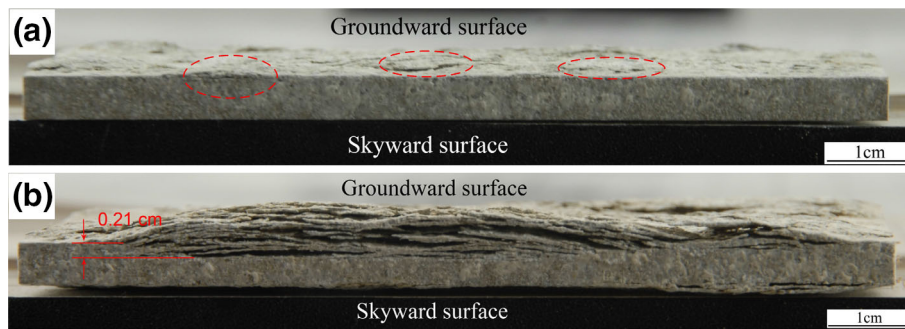
Fig. 7 Macroscopic cross-sectional morphologies of the specimens after exposure for 24 months (a) and 48 months (b)
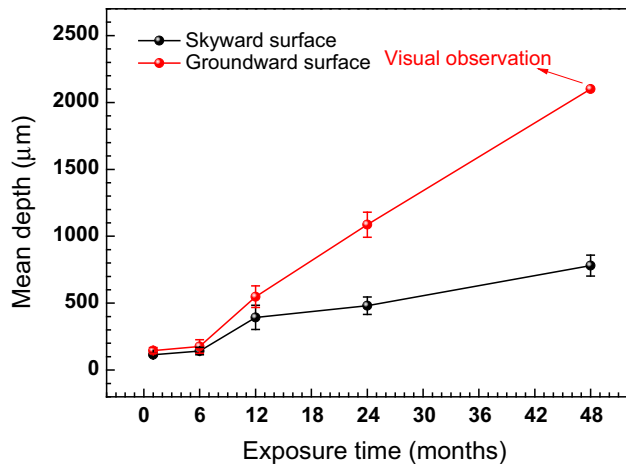

Fig. 8 Variation of the mean exfoliation depth on the skyward and groundward surfaces as a function of the exposure time

the differences become more obvious as the exposure time extends, which further confirms the different exfoliation susceptibility of the two surfaces as demonstrated in Fig. 6 and 7 and Table 2.

3.5 Corrosion Morphology

Figure 9 shows the typical corrosion morphologies after removing corrosion products from the specimens exposed for different time. Corrosion pit with a diameter of approximately 50 μm is observed on the specimen after 1 month of exposure (Fig. 9a). After 6 months, few lamellar aluminum grains begin to peel off from the substrate, leaving some cracks penetrated into the matrix (Fig. 9b). Further increasing the exposure time, ladder-laminated morphology is detected after fracturing the exfoliated structure and removing the corrosion scales (Fig. 9c and d).

4. Discussion

4.1 Exfoliation Corrosion Process and Mechanism of 2B06 Aluminum in Tropical Marine Atmosphere

As shown in Fig. 6, intergranular corrosion initiates on the aluminum surface after 1 month of exposure and exfoliation corrosion occurs after 12 month based on the fact that the uncorroded sheets has been peeled off. This phenomenon agrees with the reversed trend of corrosion rate curve at 6 months of exposure (Fig. 3b). Therefore, the process of exfoliation corrosion on 2B06 aluminum in Xisha tropical marine atmosphere can be divided into two stages, i.e., the initiation stage and the propagation stage. The initiation stage is the first 6 months during which intergranular corrosion starts at fragile sites and propagates along grain boundaries. During this stage, corrosion consumes only a small amount of the material, corresponding to the slow increase in the thickness loss in Fig. 3(a). In the propagation stage, the original sheet was seriously corroded until exhausted. Here, the thickness loss is not only attributed to the metal dissolution, but also to the non-corroded grain detachment, which explains the rapid increase in the thickness loss and corrosion rate in Fig. 3.

As shown in Fig. 6, there are obvious corrosion products located along the grain boundaries, suggesting that wedge effect from the corrosion scales plays a critical role in the exfoliation process of aluminum. In addition, there also exists some thin intergranular corrosion cracks with no evidence of corrosion product. To further investigate the exfoliation mechanism, the element distribution across the thin intergranular crack tip is examined and displayed in Fig. 10. The element composition at the crack tip is consistent with the aluminum matrix which is mainly composed of Al, Mg and Cu. This scenario verifies the absence of corrosion products at or close to the crack tip, thus suggesting the possibility of a hydrogen effect in the initiation of intergranular cracks, which is in accordance with the fact that long and thin cracks are observed far from the corrosion location (Fig. 6). Therefore, it is reasonable to speculate that exfoliation corrosion of 2B06 aluminum in tropical marine atmosphere initiates from hydrogen-assisted intergranular cracks. The volumic effect of the corrosion products, often suggested as a critical mechanism in exfoliation corrosion, subsequently lifts the cracks to create large openings.

Now that the two stages of exfoliation corrosion on 2B06 aluminum exposed to the tropical marine atmosphere have been identified, the following section is to discuss where the hydrogen comes from and how the two processes are related to each other. In previous studies, some have demonstrated that hydrogen was produced during the corrosion process. It was being trapped in distinct states in the interior of the aluminum alloy and subsequently gave rise to hydrogen embrittlement (Ref 19, 31-35). In marine atmosphere, chloride-containing electrolyte layer absorbed on the surface can easily destroy the surface film to induce pitting corrosion, and finally form the occluded cell. Thus, an acidic medium is generated in the corrosion zone due to the hydrolysis of the aluminum cations, accompanying with the hydrogen emissions (Ref 21). The formation and molecular recombination of the hydrogen atoms at or close to the grain boundaries generates sufficient pressure

to induce crack initiation. Once such cracks have initiated, they may propagate extremely fast, creating sudden contact between the aggressive medium and the fresh metallic surface, which in turn, facilitated the dissolution of the aluminum substrate. In this case, corrosion products composed of aluminum chloride/oxygen complexes which have higher molar volumes than that of aluminum could form along the gain boundaries. The corrosion products exert a significant wedging pressure between the layers of sheets to pry them apart (Fig. 6c and d).

4.2 Reasons for the Differences in Corrosion Behavior Between the Skyward and Groundward Surfaces

The differences in the corrosion behaviors between the skyward and groundward metal surfaces subjected to atmospheric exposure have been previously reported by some literatures (Ref 5, 36-38). It is generally accepted that corrosion on the groundward surface is more severe than the skyward surface. Fuente et al. (Ref 36) investigated the rust layer formed on the two surfaces of carbon steel and suggested that the longer time of wetness and the lack of rain washing which can remove the deposited saline particles on the groundward surface produced a more open structure in the corrosion products with less protective ability than those formed on the skyward surface. As for aluminum alloys, Longo (Ref 37) reported that sky-facing surfaces tended to blister more rapidly than ground-facing surfaces, especially in industrial atmospheres. Sun et al. (Ref 5) concluded that pitting corrosion mainly occurred on the groundward surface of alclad 7075 and 2024 aluminum alloy in marine atmosphere. Cui (Ref 38) investigated the pitting corrosion behavior of the AZ31

magnesium in a tropical marine atmosphere and suggested that pits on the skyward surface tended to grow in depth and exhibit a deep-hole shape attributed to the wet-dry cycles, while those on the groundward surface were inclined to spread laterally and form a shallow-dish shape because of the presence of continuous electrolyte layer.

In this work, Table 2 and Fig. 6 to 8 reveal that corrosion of the groundward surface is considerably severe than the skyward surface, showing a thicker exfoliation layer and a more serious flaking of the grain structures. These phenomena can be
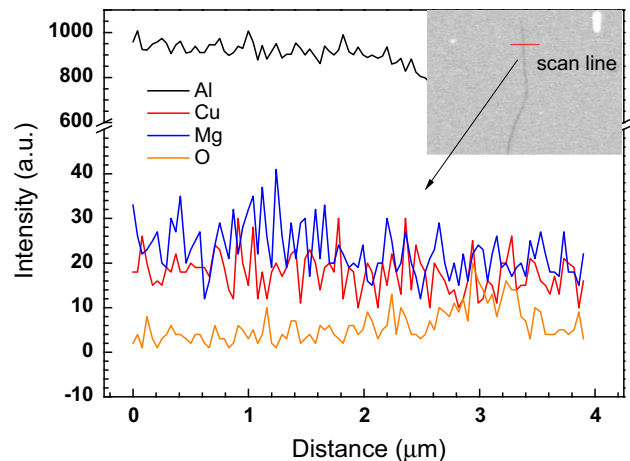

Fig. 10 Element composition near the tip area of the long and thin cracks
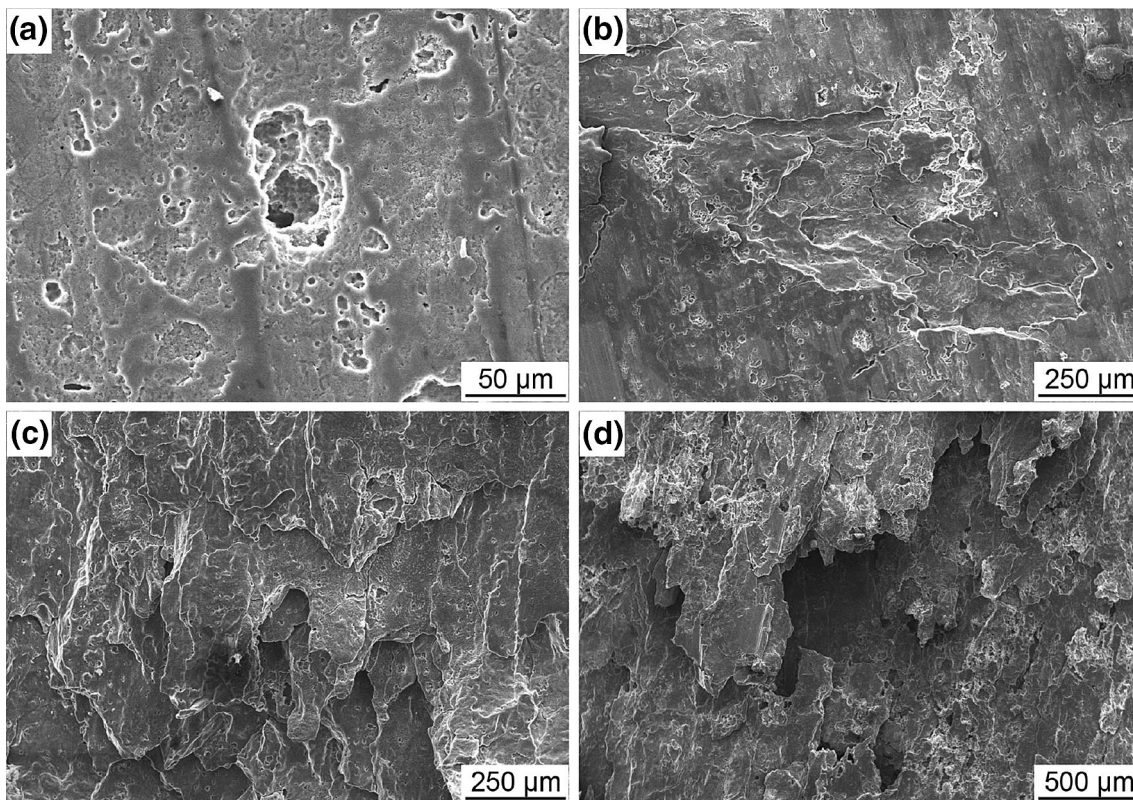

Fig. 9 Corrosion morphologies without corrosion products of the specimens after exposure for 1 month (a), 6 months (b), 12 months (c) and 24 months (d)

explained by the dissimilar exposure conditions that the skyward and groundward surfaces have experienced. Because of the sunlight and washing effect of the rainfall, wet-dry cycles would be evidently established on the skyward surface (Ref 39). In contrast, without washing effect and sun radiation, the groundward surface has a larger amount of polluted particles and a longer time of wetness, which results in a continuous absorbed electrolyte layer. Firstly, the uninterrupted exposure of the groundward surface to the salt electrolyte layer allows the chloride ions to remain in contact with the specimens whenever possible, permitting the initiation of pits and the formation of intergranular cracks during the entire exposure. On the skyward surface, however, the dry cycles inhibit the penetration of corrosion into the interior of the aluminum alloy due to the lack of corrosive medium, leading to a relatively mild exfoliation behavior. With increasing exposure time, the swelled exfoliated layer on the groundward surface can easily absorb more aggressive electrolyte which further advances the corrosion and deteriorates the metal matrix. As a result, the difference in the corrosion depths between the two surfaces becomes more obvious as shown in Fig. 8.

5. Conclusion

In this study, the atmospheric corrosion behavior is investigated for 2B06 aluminum exposed in a tropical marine atmosphere on Xisha islands for 4 years. The main conclusions are listed as follows:

(1) Exfoliation corrosion is observed in the 2B06 aluminum alloy after exposure for 6 months, which results in the rapid increase in the thickness loss and the corrosion rate.
(2) Exfoliation corrosion of 2B06 aluminum alloy in tropical marine atmosphere initiates from hydrogen-assisted intergranular cracks and propagates extensively due to the wedge effect of the corrosion products generated along the grain boundaries.
(3) Exfoliation corrosion of the groundward surface is more severe than the skyward surface due to the continuous presence of corrosive electrolyte layer caused by the absence of sun radiation rain washing effect.

References

1. K. Nisancioglu, Corrosion of Aluminum Alloys, Norwegian Institute of Technology, *SINTEF Metall. (Norway)*, 1992, **3**, p 239–259
2. T. Dursun and C. Soutis, Recent Developments in Advanced Aircraft Aluminum Alloys, *Mater. Des.*, 2014, **56**, p 862–871
3. D. De la Fuente, E. Otero-Huerta, and M. Morcillo, Studies of Long-Term Weathering of Aluminum in the Atmosphere, *Corros. Sci.*, 2007, **49**, p 3134–3148
4. B. Wang, Z. Wang, W. Han, and W. Ke, Atmospheric Corrosion of Aluminum Alloy 2024-T3 Exposed to Salt Lake Environment in Western China, *Corros. Sci.*, 2012, **59**, p 63–70
5. S. Sun, Q. Zheng, D. Li, and J. Wen, Long-Term Atmospheric Corrosion Behaviour of Aluminum Alloys 2024 and 7075 in Urban, Coastal and Industrial Environments, *Corros. Sci.*, 2009, **51**, p 719–727
6. R. Vera, D. Delgado, and B.M. Rosales, Effect of Atmospheric Pollutants on the Corrosion of High Power Electrical Conductors: Part 1. Aluminum and AA6201 Alloy, *Corros. Sci.*, 2006, **48**, p 2882–2900
7. Z. Dan, I. Muto, and N. Hara, Effects of Environmental Factors on Atmospheric Corrosion of Aluminum and its Alloys Under Constant Dew Point Conditions, *Corros. Sci.*, 2012, **57**, p 22–29
8. L. Tao, S. Song, X. Zhang, Z. Zhang, and F. Lu, Image Analysis of Atmospheric Corrosion of Field Exposure High Strength Aluminum Alloys, *Appl. Surf. Sci.*, 2008, **254**, p 6870–6874
9. T.E. Graedel, Corrosion Mechanisms for Aluminum Exposed to the Atmosphere, *J. Electrochem. Soc.*, 1989, **136**, p 204C–212C
10. L. Tao, S. Song, S. Wang, X. Zhang, M. Liu, and F. Lu, Image Analysis of Periodic Rain Accelerated Corrosion of Aeronautical Aluminum Alloys, *Mater. Sci. Eng. A*, 2008, **476**, p 210–216
11. T. Li, X. Li, C. Dong, and Y. Cheng, Characterization of Atmospheric Corrosion of 2A12 Aluminum Alloy in Tropical Marine Environment, *J. Mater. Eng. Perform.*, 2010, **19**, p 591–598
12. D.O. Sprowls, Evaluation of Exfoliation Corrosion, *ASM Handbook.*, 1987, **13**, p 242–244
13. S. Sun, Q. Zheng, D. Li, S. Hu, and J. Wen, Exfoliation Corrosion of Extruded 2024-T4 in the Coastal Environments in China, *Corros. Sci.*, 2011, **53**, p 2527–2538
14. S. Hu, S. Sun, A. Guo, X. Jia, Y. Geng, Atmospheric Corrosion Behavior of Extruded Aluminum Alloy 7075-T6 After Long-Term Field Testing in China, *Corrosion*, 2011, **67**, p 106002-106002-106010
15. M. Robinson, The Role of Wedging Stresses in the Exfoliation Corrosion of High Strength Aluminum Alloys, *Corros. Sci.*, 1983, **23**, p 887–899
16. M. Keddam, C. Kuntz, H. Takenouti, D. Schustert, and D. Zuili, Exfoliation Corrosion of Aluminum Alloys Examined by Electrode Impedance, *Electrochim. Acta*, 1997, **42**, p 87–97
17. S. Chen, K. Chen, G. Peng, L. Jia, and P. Dong, Effect of Heat Treatment on Strength, Exfoliation Corrosion and Electrochemical Behavior of 7085 Aluminum Alloy, *Mater. Des.*, 2012, **35**, p 93–98
18. L. Huang, K. Chen, S. Li, and M. Song, Influence of High-Temperature Pre-precipitation on Local Corrosion Behaviors of Al-Zn-Mg Alloy, *Scripta Mater.*, 2007, **56**, p 305–308
19. H. Kamoutsi, G. Haidemenopoulos, V. Bontozoglou, and S. Pantelakis, Corrosion-Induced Hydrogen Embrittlement in Aluminum Alloy 2024, *Corros. Sci.*, 2006, **48**, p 1209–1224
20. B. Li, Q. Pan, Z. Zhang, and C. Li, Research on Intercrystalline Corrosion, Exfoliation Corrosion, and Stress Corrosion Cracking of Al-Zn-Mg-Sc-Zr Alloy, *Mater. Corros.*, 2013, **64**, p 592–598
21. T. Marlaud, B. Malki, A. Deschamps, and B. Baroux, Electrochemical Aspects of Exfoliation Corrosion of Aluminum Alloys: The Effects of Heat Treatment, *Corros. Sci.*, 2011, **53**, p 1394–1400
22. T. Marlaud, B. Malki, C. Henon, A. Deschamps, and B. Baroux, Relationship Between Alloy Composition, Microstructure and Exfoliation Corrosion in Al-Zn-Mg-Cu Alloys, *Corros. Sci.*, 2011, **53**, p 3139–3149
23. ISO9223, Corrosion of Metals and Alloys—Corrosivity Atmospheres-Classification, 1992
24. E. Schindelholz, R. Kelly, I. Cole, W. Ganther, and T. Muster, Comparability and Accuracy of Time of Wetness Sensing Methods Relevant for Atmospheric Corrosion, *Corros. Sci.*, 2013, **67**, p 233–241
25. I.S. Cole, W. Ganther, J. Sinclair, D. Lau, and D.A. Paterson, A Study of the Wetting of Metal Surfaces in Order to Understand the Processes Controlling Atmospheric Corrosion, *J. Electrochem. Soc.*, 2004, **151**, p B627–B635
26. I.S. Cole and W. Ganther, Experimental Determination of Duration of Wetness on Metal Surfaces, *Corros. Eng. Sci. Technol.*, 2008, **43**, p 156–162
27. F. Corvo, T. Perez, Y. Martin, J. Reyes, L. Dzib, J. González-Sánchez, and A. Castañeda, Time of Wetness in Tropical Climate: Considerations on the Estimation of TOW According to ISO 9223 Standard, *Corros. Sci.*, 2008, **50**, p 206–219

28. ISO9225, Corrosion of Metals and Alloys-Corrosivity of Atmospheres-Measurement of Pollution, 1992

29. Y. Ma, Y. Li, and F. Wang, The Effect of β-FeOOH on the Corrosion Behavior of Low Carbon Steel Exposed in Tropic Marine Environment, *Mater. Chem. Phys.*, 2008, **112**, p 844–852

30. D. Kelly and M. Robinson, Influence of Heat Treatment and Grain Shape on Exfoliation Corrosion of Al-Li Alloy 8090, *Corrosion*, 1993, **49**, p 787–795

31. P. Petroyiannis, E. Kamoutsi, A. Kermanidis, S.G. Pantelakis, V. Bontozoglou, and G. Haidemenopoulos, Evidence on the Corrosion-Induced Hydrogen Embrittlement of the 2024 Aluminum Alloy, *Fatigue Fract. Eng. Mater. Struct.*, 2005, **28**, p 565–574

32. T. Zhang, W.Y. Chu, K.W. Gao, and L.J. Qiao, Study of Correlation Between Hydrogen-Induced Stress and Hydrogen Embrittlement, *Mater. Sci. Eng. A*, 2003, **347**, p 291–299

33. N. Alexopoulos and P. Papanikos, Experimental and Theoretical Studies of Corrosion-Induced Mechanical Properties Degradation of Aircraft 2024 Aluminum Alloy, *Mater. Sci. Eng. A*, 2008, **498**, p 248–257

34. H. Kamoutsi, G. Haidemenopoulos, V. Bontozoglou, P. Petroyiannis, and S.G. Pantelakis, Effect of Prior Deformation and Heat Treatment on the Corrosion-Induced Hydrogen Trapping in Aluminum Alloy 2024, *Corros. Sci.*, 2014, **80**, p 139–142

35. C. Larignon, J. Alexis, E. Andrieu, G. Odemer, and C. Blanc, The Contribution of Hydrogen to the Corrosion of 2024 Aluminum Alloy Exposed to Thermal and Environmental Cycling in Chloride Media, *Corros. Sci.*, 2013, **69**, p 211–220

36. D. De La Fuente, I. Díaz, J. Simancas, B. Chico, and M. Morcillo, Long-Term Atmospheric Corrosion of Mild Steel, *Corros. Sci.*, 2011, **53**, p 604–617

37. F.N. Longo, G.J. Durmann, Atmospheric Factors Affecting the Corrosion of Engineering Metals, ASTM STP646, PA, USA, (1978) p 97–114

38. Z. Cui, X. Li, K. Xiao, C. Dong, Z. Liu, and L. Wang, Pitting Corrosion Behaviour of AZ31 Magnesium in Tropical Marine Atmosphere, *Corros. Eng. Sci. Technol.*, 2014, **49**, p 363–371

39. T.T.N. Lan, N.T.P. Thoa, R. Nishimura, Y. Tsujino, M. Yokoi, and Y. Maeda, Atmospheric Corrosion of Carbon Steel Under Field Exposure in the Southern Part of Vietnam, *Corros. Sci.*, 2006, **48**, p 179–192